ACS OMEGA

Open Access

http://pubs.acs.org/journal/acsodf

Article

Novel Kinetic Resolution of Thiazolo-Benzimidazolines Using MAO Enzymes

Valentina Villamil, Franco Vairoletti, Ariel Tijman, Gonzalo López, Alejandro Peixoto de Abreu Lima, Cecilia Saiz, César Iglesias,* and Graciela Mahler*

Cite This: *ACS Omega* 2023, 8, 42114−42125

Read Online

ACCESS | Metrics & More | Article Recommendations | Supporting Information

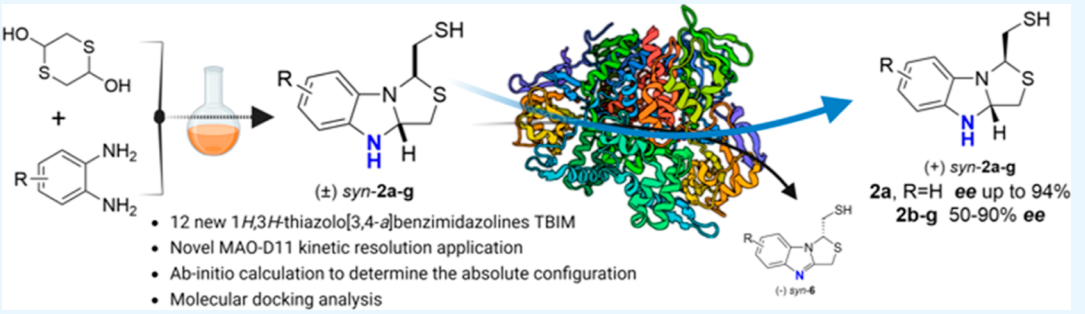

ABSTRACT: The kinetic resolution of racemic 1*H*,3*H*-thiazolo[3,4-*a*]benzimidazoline (TBIM) heterocycles was achieved using *E. coli* whole cells expressing the MAO-N D11 enzyme. Several cosolvents were screened using TBIM **2a** as the substrate. DMF was the best cosolvent, affording the pure enantiomer (+)-**2a** in 44% yield, 94% ee. The stereochemistry of TBIM was predicted by means of ab initio calculations of optical rotation and circular dichroism spectra. The reaction scope was investigated for 11 substituted (±) TBIM using an optimized protocol. The best yield and % ee were obtained for the nonsubstituted **2a**. Among the substituted compounds, the 5-substituted-TBIM showed better % ee than the 4-substituted one. The small electron donor group (Me) led to better % ee than the electron-withdrawing groups ($-NO_2$ and $-CO_2Et$), and the bulky naphthyl group was detrimental for the kinetic resolution. Docking experiments and molecular dynamics (MD) simulations were employed to further understand the interactions between MAO-N D11 and the thiazolo-benzimidazoline substrates. For **2a**, the MD showed favorable positioning and binding energy for both enantiomers, thus suggesting that this kinetic resolution is influenced not only by the active site but also by the entry tunnel. This work constitutes the first report of the enzymatic kinetic resolution applied to TBIM heterocycles.

INTRODUCTION

Heterocyclic ring systems are fundamental building blocks in medicinal chemistry and play an essential role in drug development.[1] Over 90% of new drugs contain at least one heterocyclic fragment in their structures. Among them, nitrogen-containing heterocycles are the most significant scaffolds.[2]

In recent years, imidazole and its reduced derivatives imidazolidines and imidazolines have been widely used as intermediate species in synthetic medicinal chemistry, leading to biologically active pharmacophores.[3] In particular, 2-, 3-, and 4-imidazolines are emerging privileged scaffolds with numerous applications in homogeneous catalysis[4] and in the surfactant industry (Figure 1).[5] Additionally, imidazoline-containing compounds have shown a wide range of biological and pharmacological properties, playing a central role in the treatment of numerous types of diseases. Many of the pharmacological applications of imidazoline compounds include blood pressure control and cardioprotection,[6] hyperglycemia,[7] and psychiatric disorders treatment.[8]

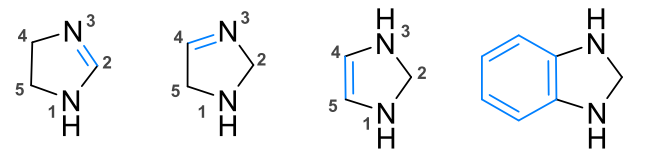

Figure 1. Structures of 2-, 3-, and 4-imidazolines and benzimidazolines.

Benzimidazolines are bicycles containing a 4-imidazoline fused with a benzene ring. This family of bicycles are widely used in organic synthesis, as reducing agents or as a hydrogen-

Received: May 9, 2023
Revised: October 6, 2023
Accepted: October 10, 2023
Published: November 1, 2023

storage material in organic reactions.[9] Furthermore, some derivatives have shown interesting antimicrobial activity.[10] Thus, benzimidazoline-containing compounds are an attractive field to be explored. Our group has recently prepared several racemic benzothiazolidines, and in order to enlarge the chemical diversity of our library, we decided to explore the synthesis of benzimidazolines.

There are a few examples of 1*H*,3*H*-thiazolo[3,4-*a*]-benzimidazolines (TBIM) synthesis through a multicomponent reaction using *o*-phenylenediamine, aryl isothiocyanates, and 4-chloro-3-oxo-butanoate.[11] In a previous work, we prepared 1*H*,3*H*-thiazolo[3,4-*b*]benzothiazolines TBTZ **1** by double condensation of 2-aminothiophenol and two molecules of 1,4-dithiane-2,5-diol.[12] Similarly, in this work, we prepare new 1*H*,3*H*-thiazolo[3,4-*a*]benzimidazolines TBIM **2** starting from 1,2-diaminoanilines and dithiane, Figure 2. These heterocycles are obtained as a racemic mixture of the *syn* diastereomer as the main product, bearing both substituents on the same side of the bicycle plane.[13]

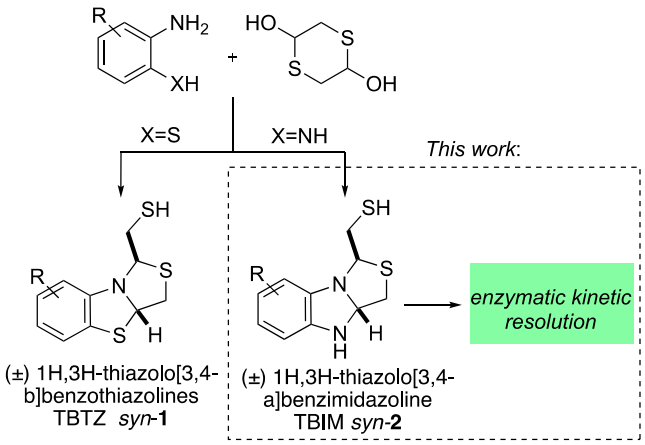

Figure 2. Synthesis of 1*H*,3*H*-thiazolo[3,4-*b*]benzothiazolines TBTZ **1** and 1*H*,3*H*-thiazolo[3,4-*a*]benzimidazolines TBIM **2**.

Since enantiomers can exhibit distinct pharmacokinetic and pharmacological properties, modern drug synthesis endeavors to produce new chiral drugs in the form of a single enantiomer.[14] Therefore, the development of efficient methods for obtaining enantiomerically pure compounds has attracted significant attention.

Several biocatalytic approaches have been described for resolving chiral amines,[15−17] including *ω*-transaminases,[18,19] amine oxidases,[20,21] P450 monooxygenases,[22,23] amine dehydrogenases,[24,25] imine reductases (IREDs),[26,27] and reductive aminases.[28] In recent years, the resolution of racemates containing amines by amino oxidase enzymes (AOs) has received particular attention for the synthesis of chiral amines in industrial biotechnology. Among these biocatalytic processes, monoamine oxidases (MAOs) have emerged as the most widely employed enzymes in biocatalysis. The multienzymatic synthesis of benzylisoquinoline alkaloids was facilitated using MAO enzymes from *Micrococcus luteus*.[29] Nevertheless, MAO enzymes from *Aspergillus niger* (MAO-N) and its variants have become the most commonly used for such applications.

MAO enzymes facilitate the oxidation of amines to imines using molecular oxygen as the oxidizing agent, as illustrated in Figure 3.[30,31] The native MAO enzymes show poor

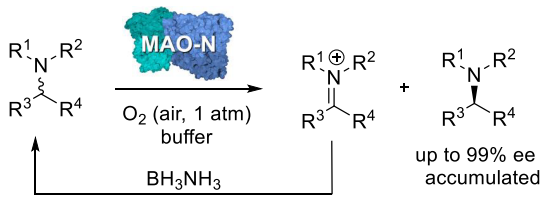

Figure 3. General scheme for dynamic kinetic resolution or deracemization: MAO-N catalyzes the oxidation of primary, secondary, and tertiary amines, followed by chemical nonselective reduction of imines by BH_3−NH_3.

enantioselectivity, rendering them ineffective in resolving chiral amines. However, by utilizing directed mutagenesis, Turner et al. have developed a set of MAO variants from *A. niger*, named D3, D5, D9, D10, and D11, which have proven effective for resolving a wide range of chiral primary, secondary, and tertiary amines, Figure 4.[20] When a chemical reducing agent such as

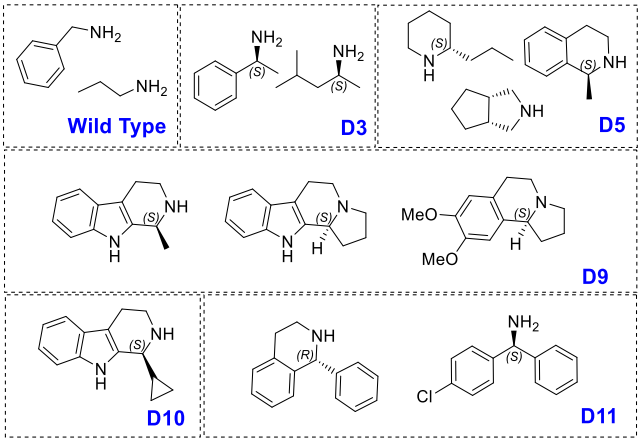

Figure 4. Examples of the dynamic kinetic resolution of different substrates using MAO-N variants.

BH_3−NH_3 is employed, the imines formed during catalysis can be reduced, leading to oxidation−reduction cycles with the enzyme, and thus achieving a dynamic kinetic resolution or deracemization, with yields as high as 100%, as depicted in Figure 3.[30,32]

In order to explore a suitable methodology to obtain the enantiomerically pure heterocycles TBTZ **1** and TBIM **2** under mild conditions, we envisioned that the use of MAO enzymes could be a useful approach. To the best of our knowledge, this methodology has not been used so far for the kinetic resolution of benzimidazolines nor benzothiazolines.

RESULTS AND DISCUSSION

Synthesis of TBTZ 1 and TBIM 2. Racemic TBTZ **1a** and TBIM **2a−g** were obtained in a single step by double cyclization of 2-aminothiophenol **3a** or 2-aminoanilines **4a−g**, respectively, and 1,4-dithiane-2,5-diol **5** in yields ranging from 49 to 85%, Table 1.

When using 5-substituted-2-aminoanilines, two possible isomers at the 4- and 5-positions are obtained. After the first cyclization, a benzimidazoline intermediate is formed, bearing two nitrogen atoms able to react with a second molecule of aldehyde. The nature of the R substituent leads to a difference in the nucleophilicity between N^1 and N^2, determining the 4/5-TBIM ratio. Electron-withdrawing groups decrease the

https://doi.org/10.1021/acsomega.3c03223
ACS Omega 2023, 8, 42114−42125

Table 1. Synthesis of (±)-TBTZ 1 and (±)-TBIM 2, Starting from 2-Aminothiophenol 3a or 2-Aminoanilines 4a−g, Respectively, and 1,4 Dithiane-2,5-Diol 5

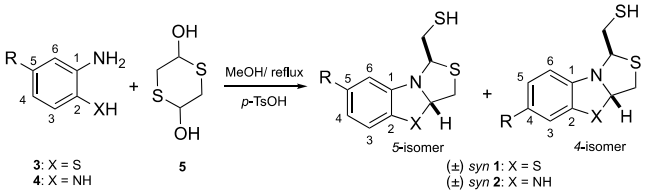

entry	compound	X	R	total yield (%)[a]	ratio-4/-5[b]
1	**1a**	S	H	85[12]	
2	**2a**	NH	H	58	
3	**2b**	NH	4-5-naphthyl	71	
4	4-**2c**	NH	$-CH_3$	58	6/4
5	5-**2c**	NH	$-CH_3$		
6	4-**2d**	NH	$-CO_2Et$	49	3/7
7	5-**2d**	NH	$-CO_2Et$		
8	4-**2e**	NH	$-NO_2$	83	3/7
9	5-**2e**	NH	$-NO_2$		
10	4-**2f**	NH	−F	75	7/3
11	5-**2f**	NH	−F		
12	4-**2g**	NH	−Br	69	7/3
13	5-**2g**	NH	−Br		

[a]Yields correspond to purified compounds by column chromatography on flash SiO_2. [b]The ratio was calculated by ^1H NMR.

nucleophilicity of N^2 with respect to N^1, giving the 5-substituted compound (5-TBIM) as the main product, see Table 1, entries 6−9. On the other hand, electron-donating groups increase the nucleophilicity of N^2 compared to N^1, affording the compound 4-TBIM as the main product, see Table 1, entries 4 and 5.

Analytical-Scale Screening Using *E. coli* Whole Cells. In order to evaluate the enantioselectivity of the MAO enzyme toward the resolution of TBTZ **1** and TBIM **2**, the simplest unsubstituted substrates **1a** and **2a** were selected as a model to study the optimal deracemization conditions. We hypothesize the formation of the imine oxidation product and the enantiopure TBTZ or TBIM, as shown in Scheme 1.

Scheme 1. Proposal for the Resolution of Heterocycles 1a and 2a Using MAO-N Variants

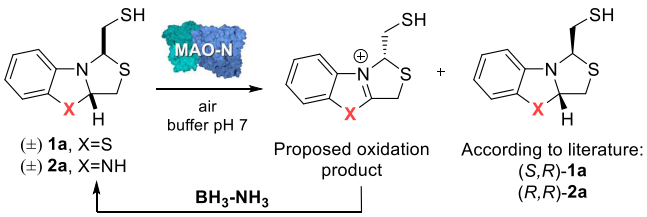

Thus, the racemic mixtures were subjected to a deracemization protocol using *E. coli* whole cells expressing three different MAO-N variants (D5, D9, and D11) to compare the activity and enantioselectivity. Reactions were carried out in phosphate buffer (0.1 M, pH = 7) and the substrate at 4 mM concentration, using BH_3-NH_3 (4 equiv) as the reducing agent. Aliquots were taken at different times and diluted for chiral HPLC analysis. Yields and enantiomeric excess (% ee) were calculated, Table 2. According to literature, the expected isolated enantiomer should be (*S*,*R*)-**1a** and (*R*,*R*)-**2a** since the substrates are voluminous.[30]

Table 2. Analytical-Scale Screening for the Enzymatic Resolution of TBTZ 1a and TBIM 2a Using Whole Cells (*E. coli*) Expressing MAO-N Variants: D5, D9, and D11[a]

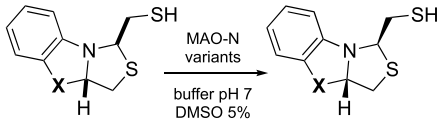

substrate	time	4 h		48 h	
	MAO-N variant	% ee[b]	yield (%)[c]	% ee[b]	yield (%)[c]
(*S*,*R*)-**1a**	D5	0	46	0	26
	D9	0	47	0	22
	D11	0	42	0	27
(*S*,*S*)-**2a**	D5	14	42	56	11
	D9	28	37	18	9
	D11	90	31	64	2

[a]Conditions: cells 1 g/mL, phosphate buffer 0.1 M pH 7, [substrate] = 4 mM, BH_3NH_3, DMSO 5%, 37 °C. [b]Calculated by chiral HPLC. [c]Calculated by chiral HPLC using an external standard.

Despite no resolution was found for TBTZ **1a** using the three variants, all of them resulted to be enantioselective for TBIM **2a**. In particular, the D11 variant showed the best result, providing the optically enriched product in 31% yield with excellent enantiomeric excess (90%) after 4 h, Table 2. A longer reaction time (48 h) decreased both the yield and % ee. This result could be explained if the oxidation rate for (*S*,*S*)-**2a** is higher than that for its enantiomer (*R*,*R*)-**2a**. Over time, when the preferred enantiomer is consumed, the enzyme continues oxidizing the remaining enantiomer, decreasing the % ee.

Attempts to scale-up the resolution reaction with whole cells led to lower % ee, so we decided to employ the purified enzyme MAO-N D11[33] for the resolution of TBIM. Although cleaner reactions were carried out, the optically enriched product was obtained with 46% ee. Thus, we decided to continue optimizing the reaction employing *E. coli* whole cells since enzyme purification is a time-consuming approach and did not improve the % ee or the yield of the reaction.

Solvent Screening. We hypothesized that the unsuccessful scale up could be due to the slight solubility of the compounds in the reaction media; the organic cosolvent used could have a strong influence in both the yield and the % ee; thus, its effect was studied. The reaction was performed with **2a** and *E. coli* whole cells expressing MAO-N D11 as a biocatalyst, and several organic cosolvents at different concentrations were screened. The results (yield and % ee) are shown in Table 3.

The results indicated a strong influence of the cosolvent on the % ee. The best results were achieved using 5% DMF, affording **2a** in 44% yield, 94% ee after 2 h (Table 3, entry 7 and Figure S15A,B). This may be due to a higher solubility of the compound in DMF, increasing the availability of the compound in the reaction medium. Even though longer reaction times improved the % ee, the reaction yields decreased notoriously (Table 3, entries 8 and 9), probably due to chemical oxidation or heterocycle ring-opening in the reaction media.

https://doi.org/10.1021/acsomega.3c03223
ACS Omega 2023, 8, 42114−42125

Table 3. Analytical-Scale Screening of Cosolvents for the Enzymatic Resolution of TBIM 2a Using *E. coli* Whole Cells Expressing MAO-N D11[a]

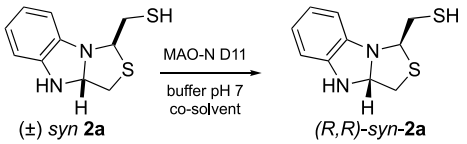

(±) *syn* **2a** (*R,R*)-*syn*-**2a**

entry	solvent	time (h)	% ee[b]	yield (%)[c]
1	DMSO 5%	2	82	37
2		4	86	23
3		6	84	9
4	DMSO 10%	2	83	34
5		4	85	19
6		6	80	11
7	DMF 5%	2	94	44
8		4	94	26
9		6	94	18
10	MeOH 5%	2	68	41
11		4	82	23
12		6	80	15
13	PhMe 5%	2	68	40
14		4	60	23
15		6	68	12

[a]Conditions: cells 1 g/mL, phosphate buffer (0.1 M, pH 7), [*syn*-**2a**] = 4 mM, co-solvent 5−10%, BH_3NH_3, 37 °C. [b]Calculated by chiral HPLC. [c]Calculated by chiral HPLC using an external standard.

The lowest % ee were obtained using toluene as cosolvent, probably because a biphasic system is formed and compound **2a** remains in the organic layer.

On the other hand, the effect of the additive BH_3NH_3 was evaluated in the kinetic resolution using the optimized conditions (DMF 5% as cosolvent). The results showed that its use smoothly improved the reaction yields, see Table S1. The reductive environment probably avoids thiol oxidation, which could be accelerated by H_2O_2 formation during the MAO-N-catalyzed biotransformation.

Reaction Scale-Up. Once the best reaction conditions were established, the reaction was scaled-up for the resolution of (±)-**2a** using *E. coli* whole cells expressing the MAO-N D11 enzyme in buffer at pH 7 and 5% DMF for 2 h. Under these conditions, the (+)-**2a** enantiomer was isolated in 35% yield and 89% ee, together with compound (−)-**6**, as shown in Scheme 2 and Figure S1.

Scheme 2. Scale-Up of the Kinetic Resolution Reaction of 2a Using *E. coli* Cells Expressing MAO-N D11 in Phosphate Buffer pH 7 and 5% DMF, BH_3NH_3, 2 h

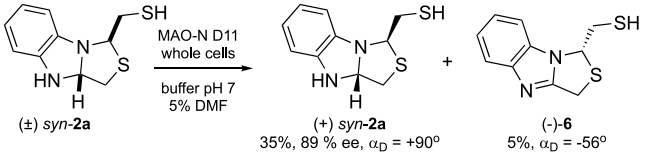

(±) *syn*-**2a** (+) *syn*-**2a** 35%, 89 % ee, α_D = +90° (-)-**6** 5%, α_D = -56°

The 1*H*,3*H*-thiazolo[3,4-*a*]benzimidazole (−)-**6** was identified as the oxidation product of the reaction, in which the aromatic secondary amine present in **2a** is oxidized by the MAO enzyme. This result supports that benzothiazoline **1a**, lacking the aromatic secondary amine, cannot be resolved using this methodology. In addition, since the reduction of an aromatic benzimidazole is challenging, a dynamic kinetic resolution using BH_3−NH_3 as a reducing agent was not possible.

The synthesis of racemic thiazolo-benzimidazoles similar to **6** is described in literature using *o*-phenylenediamines, 2-mercaptoacetic acid, and different aldehydes.[34−36] Interestingly, some thiazolo-benzimidazoles derivatives were reported as potent inhibitors of human immunodeficiency virus replication in a variety of human cell lines.[37]

Attempts to obtain compound **6** by chemical oxidation of TBIM **2a** using MnO_2 in MeOH failed, and decomposition of the starting material was observed. The biocatalytic methodology herein described allowed us to isolate the enantiopure thiazolo-benzimidazole (−)-**6**. Further optimization of the reaction conditions could provide a useful approach for the enantioselective preparation of this type of compounds.

Mechanism Insights: Oxidation Mechanism Proposal. The oxidation mechanisms of monoamine oxidases (MAOs) have been widely studied for the MAO-A and MAO-B isoenzymes, commonly found in mammals. In the literature, several mechanisms have been proposed, depending on the enzyme variant and the substrate,[38,39] including radical mechanisms and hydride transfers between the FAD cofactor and the substrate.[40]

Recently, Turner et al. reported the oxidation of indolines to indoles using MAO-N D11 via a mechanism that involved a transfer of hydrides from the substrate to FAD.[41] Based on this observation, we suggest a similar mechanism for the oxidation of TBIM using MAO-N D11, as shown in Figure 5.

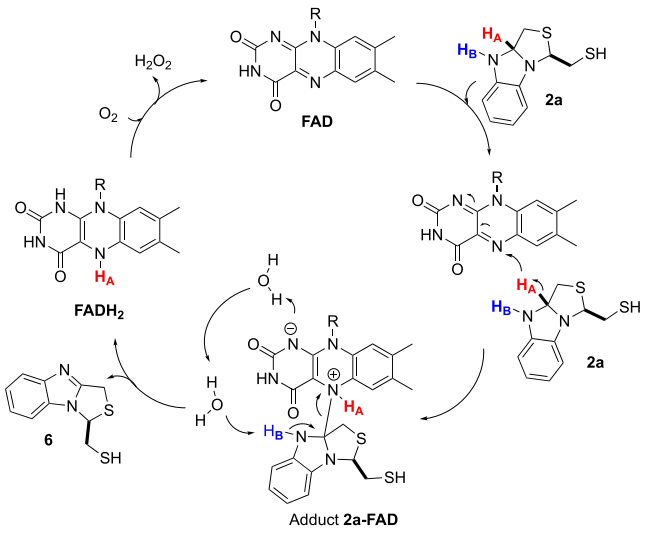

Figure 5. Proposed oxidation mechanism of TBIM **2a** by MAO-N.

In the proposed mechanism, the FAD cofactor of the enzyme abstracts a hydride from the acetalic position of TBIM **2a** (H_A), forming a TBIM-FAD adduct. Further details regarding the intermediate steps of this stage have yet to be elucidated. Subsequently, deprotonation of H_2O by the flavin is followed by protonation of a second H_2O molecule from the active site, leading to the donation of the H_B proton by N and the formation of the C=N bond (Figure 5, adduct **2a-FAD**). This results in the release of TBIM oxidation product **6** and the formation of $FADH_2$, which is reconverted by O_2 into FAD, allowing a new catalytic cycle.

https://doi.org/10.1021/acsomega.3c03223
ACS Omega 2023, 8, 42114−42125

Determination of the Absolute Configuration. Once the pure enantiomer (+)-**2a** was obtained, different methodologies were explored to determine its absolute configuration. Since compound **2a** is an oil at room temperature, we attempted to derivatize it by preparing a thioester to obtain a crystalline solid whose structure could be resolved by X-ray diffraction.

First, the thioester **7** was synthesized from the racemic mixture (±)-**2a**, using *p*-chlorobenzoic acid and HBTU as coupling agent, in 42% yield, Scheme 3A.

Scheme 3. (A) Synthesis of Thioester 7. (B) ORTEP: Molecular Structure of the Racemic Mixture (±)-7

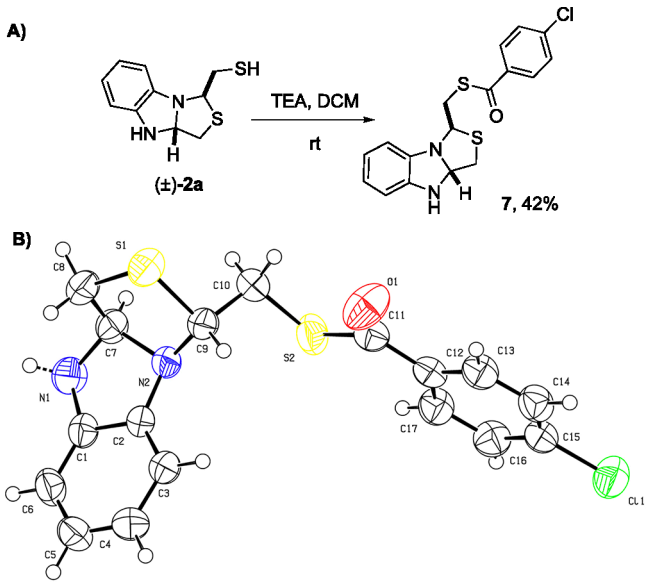

The crystal structure of **7** was obtained after the slow evaporation of CH_2Cl_2/*n*-hexanes (1:9) at room temperature and then determined by single-crystal X-ray diffraction methods. The molecular structure allowed us to confirm the relative *syn* configuration of **2a**. The ORTEP view of the compound is shown in Scheme 3B.

Then, enantiomer (+)-**2a** was derivatized using the aforementioned procedure. The derivative was subjected to similar crystallization conditions using slow evaporation of CH_2Cl_2/*n*-hexanes (1:9) at room temperature. However, crystals could not be isolated. This may be due to differences in the crystal morphology and crystal growth between the pure enantiomer and the racemic mixture.[42]

Computational Prediction of Chiroptical Properties. In order to explore an alternative methodology for the determination of the absolute configuration of the (+)-**2a** isomer, theoretical calculation studies were performed. The absolute configuration was predicted from the comparison of theoretical and experimental optical rotation values (OR) and the electronic circular dichroism (ECD) spectrum.[43,44]

Optical Rotation. First, the theoretical α_D value of both enantiomers (*R*,*R*)-**2a** and (*S*,*S*)-**2a** was calculated. After a conformational search for each enantiomer, the most favorable conformations were submitted to Gaussian16 for DFT optimization and optical rotation prediction (see the Experimental Section for details). The values for the different conformations of each enantiomer were combined through Boltzmann averaging using the Gibbs free energy calculated during the DFT optimization procedure.

The theoretical values of α_D were +46 for (*R*,*R*)-**2a** and −61 for the (*S*,*S*)-**2a** isomer. The isolated isomer (+)-**2a** has an experimental α_D = +90°; thus, the positive value suggests that (+)-**2a** is the (*R*,*R*)-enantiomer.

Electronic Circular Dichroism. To obtain additional structural information and confirm these results, the theoretical and experimental ECD spectra of the isolated isomer (+)-**2a** were determined.

The experimental ECD spectrum was recorded in the range 230−400 nm, and the values of $\Delta\varepsilon$ were calculated; see Supporting Information, Table S2. For ECD spectra calculations, a time-dependent DFT calculation was performed over the three most favorable conformations of each enantiomer with the same functional and basis set used for optical rotation. Thirty excited states and their electronic transition intensities and rotatory strengths were predicted. Boltzmann averaging was used to combine the results of the three conformations.

The comparison between the experimental and theoretical spectra of both enantiomers is shown in Figure 6. Both in the

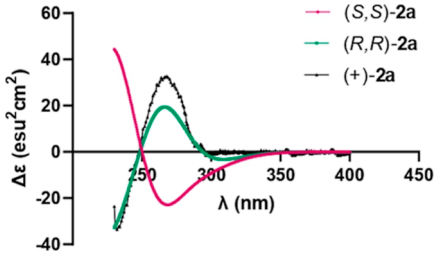

Figure 6. ECD spectra: experimental (+)-**2a** (black); calculated (*R*,*R*)-**2a** (green); and calculated (*S*,*S*)-**2a** (pink).

experimental ECD (black) and in the theoretical spectrum for the (*R*,*R*) isomer (green), a negative peak close to 230 nm and a positive peak close to 270 nm are present. These results, in accordance with the optical rotation studies, also suggest that the isolated enantiomer is the (*R*,*R*) isomer.

Kinetic Resolution Reaction Scope. Once the reaction conditions were optimized, the substrate scope was explored. A series of TBIM bearing different substituents on the aromatic ring were subjected to a kinetic resolution with MAO-N D11 under the optimized conditions. The results are shown in Table 4 (Supporting Information, Figure S16).

The results of the study indicated that the nonsubstituted TBIM **2a** achieved the best results, obtaining (*R*,*R*)-**2a** in 44% yield and 94% ee after 2 h. On the other hand, substitutions at the aromatic ring in TBIM **2b**−**g** led to a decrease in the % ee.

Overall, the 5-substituted TBIM gave better % ee than the 4-TBIM, probably due to steric hindrance or electronic effects.

The electronic or steric nature of the substituent present in the benzene ring of TBIM seems to have an impact on the % ee. The best results were obtained for compounds 4-/5-**2c** bearing a small electron donor group (Me) with 72 and 76% ee, respectively, after 2 h. The presence of the bulky naphthyl group and the electron-withdrawing groups (−CO_2Et and −NO_2) were deleterious for the kinetic resolution reaction, and no oxidation product was detected. Degradation products were not detected under the chromatographic conditions used.

Compounds 4/5-**2f** (F) afforded moderate results; pure enantiomers were obtained in 50 and 56% ee, respectively,

https://doi.org/10.1021/acsomega.3c03223
ACS Omega 2023, 8, 42114−42125

Table 4. Analytical-Scale Screening for the Enzymatic Resolution of TBIM 2b−g Using *E. coli* Whole Cells Expressing MAO-N D11[a]

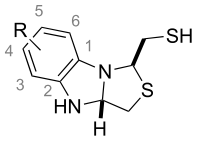

		time (h)							
		1		2		4		8	
TBIM	R	yield (*R*,*R*) %[b]	% ee[c]	yield (*R*,*R*) %[b]	% ee[c]	yield (*R*,*R*) %[b]	% ee[c]	yield (*R*,*R*) %[b]	% ee[c]
2a	H	39	92	28	94	19	94	4	92
2b	4-5-naphthyl	47	0	45	0	44	0	43	0
4-**2c**	CH_3	31	70	15	72	8	78	2	64
5-**2c**		26	72	10	76	5	74	3	40
4-**2d**	$-CO_2Et$	43	0	33	0	23	0	16	0
5-**2d**		41	0	35	0	28	0	22	0
4-**2e**	$-NO_2$	48	0	45	0	42	0	31	0
5-**2e**		49	8	48	10	46	16	37	14
4-**2f**	−F	36	50	23	44	14	44	2	46
5-**2f**		15	56	0		0		0	
4-**2g**	−Br	42	0	37	0	18	0	11	0
5-**2g**		22	26	11	30	6	90	0	

[a]Conditions: cells 1 g/mL, phosphate buffer 0.1 M pH 7, BH_3NH_3, DMF 5%, 37 °C. [b]Calculated using chiral HPLC using an external standard. [c]Calculated using chiral HPLC.

after 1 h of reaction. Notably, in the case of compound 5-**2f** (F), neither enantiomer was observed after 4 h, likely due to the rapid chemical degradation of the compound in the reaction medium.

No resolution was achieved for compound 4-**2g** (Br), while compound 5-**2g** (Br) was obtained with an ee of 90% but in a low yield (6%) after 4 h of the reaction. Although a good enantioselectivity was obtained at longer reaction times, probably the instability of the compounds in the reaction medium was the cause of the low yields.

Docking Experiments. In order to gain deeper insights into the observed enantioselectivity of MAO-N D-11, a multistep in silico analysis was performed over both enantiomers of substrate (+) and (−) *syn*-**2a**, which included flexible docking, molecular dynamics (MD) simulations, and free energy calculations. The most favorable docking positions were selected based on mechanistic considerations and were then subjected to 100 ns of free and steered MD simulations. Finally, MM-GBSA and MM-PBSA free energy calculations were performed over the clusterized trajectory of the MDs to provide a comprehensive understanding of the results.

The results indicate that both enantiomers (*R*,*R*)-**2a** and (*S*,*S*)-**2a** are optimally positioned for the reaction and have negative binding energies of −39.0 ± 3.2 and −31.9 ± 3.1 kcal/mol (MM-GBSA) and suggest that the two stereo-complementary molecules have a high binding affinity. Only a slight advantage was observed for the *SS* enantiomer regarding the positioning angle of the H_A hydrogen in relation to the nitrogen of the FAD. In addition, the *RR* enantiomer shows a subtle steric hindrance at the thiol chain with the amino acid PHE382, something that does not occur with the *SS* enantiomer (Supporting Information, Figure S17). However, experimentally, it was observed that one of the enantiomers reacted more slowly. From this analysis, it can be concluded that the observed enantioselectivity at 4 and 24 h of the reaction may be due to the transition speed of the enantiomers through the entry tunnel of the active site. The steric hindrance toward the *RR* enantiomer may also affect the behavior of the molecule inside the active site, reducing its binding capacity and increasing the reaction time.

The MAO-N entry tunnel has been mutated in several studies, proving to be a limiting factor in substrate specificity. In this case, the results obtained from the MD simulations and energy calculations seem to indicate that the physicochemical properties of the tunnel and not the active site might be crucial for the observed reaction rate. This observation supplies an interesting target to improve substrate specificity in the future with this type of compounds.

Flexible docking analyses for all the derivatives **2b−g** were performed. Docking analysis of **2b** (naphthyl) and **2d** (CO_2Et) showed that clusters with the negative energy of binding did not provide a suitable structure from a mechanistic point of view, which correlates with the lack of experimental activity. Additionally, a clear increase in energy binding was observed in the entry regions of the tunnel, indicating steric hindrance that could prevent entry into the active site.

CONCLUSIONS

A series of 12 new 1*H*,3*H*-thiazolo[3,4-*a*]benzimidazolines TBIM **2a−g** compounds were synthesized through the double condensation of 1,2-aminoanilines and dithiane, with yields ranging from 49 to 85%. In order to resolve the racemic mixture, the use of MAO enzymes was investigated.

Multiple conditions were evaluated, including different MAO-N variants, reaction times, and cosolvents. The optimal resolution conditions were achieved using the MAO-N D11 variant and 5% DMF as cosolvent after 2 h of reaction. This approach was effective for the enantiomeric resolution of TBIM **2a**, but not for the sulfur analogue TBTZ **1a**.

The reaction scope was studied using different substituted TBIM **2a−g**. The best result was achieved for the non-substituted TBIM **2a**, yielding the pure enantiomer (+)-**2a**

https://doi.org/10.1021/acsomega.3c03223
ACS Omega 2023, 8, 42114−42125

with 94% ee and 44% yield at 4 mM. Additionally, the enantiomerically pure 1*H*,3*H*-thiazolo[3,4-*a*]benzimidazole (−)-**6** was isolated as the oxidation product, providing a new methodology for its enantioselective preparation, to be optimized. The formation of this benzimidazole avoided the dynamic resolution of the racemic mixture. This result also explains why benzothiazoline **1a** could not be resolved using MAO enzymes.

The absolute configuration was determined by measuring the α_D value and the ECD spectrum. The results were compared to those obtained by theoretical calculations, indicating that the absolute configuration of the isolated enantiomer is (*R*,*R*). Additionally, docking studies demonstrate that the *SS* enantiomer has only a slight advantage in positioning in the active site, indicating that the entry tunnel must account for the observed differences in reaction rates.

In summary, a new application of MAO-N D11 for the resolution of 1*H*,3*H*-thiazolo[3,4-*a*]benzimidazoline was achieved.

EXPERIMENTAL SECTION

General Procedure for the Synthesis of 1*H*,3*H*-Thiazolo[3,4-*a*]benzimidazolines (TBIM 2). To a stirred solution of 2-diaminoaniline (1 mmol) in EtOH (10 mL) were added 1,4-dithiane-2,5-dithiol (1.2 mmol) and catalytic *p*-TsOH acid (0.1 mmol). The mixture was heated at reflux for 1 h. The solvent was then removed under reduced pressure. The crude was poured into water (30 mL), extracted with EtOAc (3 × 50 mL), dried (Na_2SO_4), and filtered. The organic layer was evaporated under reduced pressure. The crude reaction mixture was purified by column chromatography on flash silica gel using *n*-hexanes/EtOAc, to obtain the TBIM compounds.

*(3a,4-Dihydro-1H,3H-benzo[4,5]imidazo[1,2-c]thiazol-1-yl)methanethiol (**2a**).* Prepared starting from *o*-phenylenediamine (200 mg, 0.925 mmol) and purified with *n*-hexanes/EtOAc 8:2 to give **2a** (112 mg, 58%) as a colorless oil: ^{1}H NMR: δ 6.81 (m, 3H), 6.71 (dd, J = 6.1, 2.6 Hz, 1H), 5.35 (dd, J = 7.5, 5.4 Hz, 1H), 4.98 (dd, J = 8.9, 4.7 Hz, 1H), 4.18 (br, 1H), 3.16 (dd, J = 10.6, 5.4 Hz, 1H), 2.91 (ddd, J = 13.8, 8.9, 6.3 Hz, 1H), 2.83 (dd, J = 10.6, 7.5 Hz, 1H), 2.70 (ddd, J = 13.6, 10.6, 4.7 Hz, 1H), 1.90 (dd, J = 10.6, 6.3 Hz, 1H); ^{13}C RMN: δ 140.8, 138.0, 121.9, 121.8, 111.9, 110.0, 83.1, 71.5, 38.9, 33.9; IR (NaCl) ν: 1620, 1495, 1406, 1292, 1250, 1115, 740, 695 cm^{-1}; HRMS (ESI) m/z: calcd for $C_{10}H_{12}N_2S_2$ [M + Na]$^+$ 247.0340; found, 247.0341.

*(3a,4-Dihydro-1H,3H-naphtho[2′,3′:4,5]imidazo[1,2-c]-thiazol-1-yl)methanethiol (**2b**).* Prepared starting from 2,3-diaminonaphthalene (160 mg, 1 mmol) and purified with *n*-hexanes/EtOAc 8:2 to give **2b** (194.5 mg, 71%); brown solid, mp 165−173 °C; ^{1}H NMR: δ 7.62 (m, 1H), 7.56 (m, 1H), 7.23 (m, 2H), 7.04 (s, 1H), 6.91 (s, 1H), 5.48 (dd, J = 7.6, 5.2 Hz, 1H), 5.08 (dd, J = 8.8, 4.7 Hz, 1H), 4.48 (br, 1H), 3.19 (dd, J = 10.6, 5.2 Hz, 1H), 3.00 (ddd, J = 14.9, 8.7, 6.4 Hz, 1H), 2.82 (dd, J = 10.5, 7.4 Hz, 1H), 2.78 (ddd, J = 13.8, 10.8, 5.3 Hz, 1H), 1.93 (dd, J = 10.6, 6.3 Hz, 1H); ^{13}C NMR: δ 141.3, 139.1, 131.2, 130.7, 126.6, 126.2, 123.8, 123.8, 105.5, 104.7, 83.0, 70.8, 39.1, 33.8; IR (NaCl) ν: 3346, 2924, 1633, 1599, 1472, 1433, 1375, 1314, 1265, 959, 853, 741 cm^{-1}; HRMS (ESI) m/z: calcd for $C_{14}H_{13}N_2S_2$ [M − H]$^-$ 273.0520; found, 273.0521.

*(6-Methyl-3a,4-dihydro-1H,3H-benzo[4,5]imidazo[1,2-c]-thiazol-1-yl) Methanethiol (4-**2c**) and (7-Methyl-3a,4-dihydro-1H,3H-benzo[4,5]imidazo[1,2-c]thiazol-1-yl)-methanethiol (5-**2c**).* Prepared starting from 4-methyl-*o*-phenylenediamine (120 mg, 1 mmol) and purified with CH_2Cl_2/*n*-hexanes 1:1 to give a mixture of isomers 4-**2c** and 5-**2c**, 0.138 g, 58%, (7:3).

4-**2c**: (40.5 mg, 17%): colorless oil; ^{1}H NMR: δ 6.66 (m, 2H), 6.54 (t, J = 11.2 Hz, 1H), 5.33 (dd, J = 7.1, 5.5 Hz, 1H), 4.93 (dd, J = 9.0, 4.7 Hz, 1H), 4.13 (br, 1H), 3.16 (dd, J = 10.7, 5.4 Hz, 1H), 2.89 (ddd, J = 13.7, 9.0, 6.2 Hz, 1H), 2.83 (dd, J = 10.7, 7.3 Hz, 1H), 2.68 (ddd, J = 13.6, 10.6, 4.7 Hz, 1H), 2.24 (s, 3H), 1.91 (dd, J = 10.6, 6.2 Hz, 1H); ^{13}C NMR: δ 138.6, 138.3, 131.7, 122.0, 112.9, 109.8, 83.4, 72.1, 39.0, 33.9, 21.2; IR (NaCl) ν: 3346, 1497, 1458, 1373, 1265, 1217, 1150, 760 cm^{-1}; HRMS (ESI) m/z: calcd for $C_{11}H_{14}N_2NaS_2$ [M − H]$^-$ 261.0496; found, 261.0500.

5-**2c**: (27.9 mg, 12%): colorless oil; ^{1}H NMR: δ 6.63 (m, 3H), 5.32 (dd, J = 7.7, 5.5 Hz, 1H), 4.97 (dd, J = 9.0, 4.7 Hz, 1H), 3.14 (dd, J = 10.6, 5.4 Hz, 1H), 2.90 (ddd, J = 13.6, 9.0, 6.2 Hz, 1H), 2.81 (dd, J = 10.6, 7.7 Hz, 1H), 2.69 (ddd, J = 13.6, 10.6, 4.6 Hz, 1H), 2.28 (d, J = 0.7 Hz, 3H), 1.91 (dd, J = 10.6, 6.2 Hz, 1H); ^{13}C NMR: δ 141.4, 135.6, 132.2, 122.1, 112.5, 110.9, 83.4, 77.5, 71.3, 38.7, 34.0, 21.4; IR (NaCl) ν: 3344, 1492, 1458, 1373, 1260, 1217, 1208, 1155, 760 cm^{-1}; HRMS (ESI) m/z: calcd for $C_{11}H_{14}N_2NaS_2$ [M − H]$^-$ 261.0496; found, 261.0500.

*Ethyl 1-(Mercaptomethyl)-3a,4-dihydro-1H,3H-benzo-[4,5]imidazo[1,2-c]thiazole-6-carboxylate (4-**2d**) and Ethyl 1-(Mercaptomethyl)-3a,4-dihydro-1H,3H-benzo[4,5]-imidazo[1,2-c]thiazole-7-carboxylate (5-**2d**).* Prepared starting from ethyl 3,4-diaminobenzoate (180 mg, 1 mmol) and purified with *n*-hexanes/EtOAc 8:2 to give a mixture of isomers 4-**2d** and 5-**2d** 0.145 g, 49%, (3:7).

4-**2d**: (35.6 mg, 12%), yellow oil; ^{1}H NMR: δ 7.61 (dd, J = 8.1, 1.6 Hz, 1H), 7.31 (d, J = 1.5 Hz, 1H), 6.76 (d, J = 8.1 Hz, 1H), 5.42 (dd, J = 7.8, 5.3 Hz, 1H), 5.00 (dd, J = 8.8, 4.6 Hz, 1H), 4.31 (q, J = 7.1 Hz, 2H), 3.16 (dd, J = 10.6, 5.3 Hz, 1H), 2.91 (ddd, J = 13.8, 8.8, 6.6 Hz, 1H), 2.80 (dd, J = 10.6, 7.8 Hz, 1H), 2.72 (ddd, J = 13.8, 10.5, 4.7 Hz, 1H), 1.86 (dd, J = 10.5, 6.5 Hz, 1H), 1.35 (t, J = 7.1 Hz, 3H); ^{13}C NMR: δ 166.8, 144.7, 138.2, 125.0, 124.0, 111.9, 108.4, 83.2, 70.2, 60.7, 38.8, 33.7, 14.5; IR (NaCl) ν: 2976, 2926, 1700, 1603, 1497, 1450, 1366, 1285, 1210, 1103, 1020, 765 cm^{-1}; HRMS (ESI) m/z: calcd for $C_{13}H_{16}N_2NaO_2S_2$ [M + Na]$^+$ 319.0545; found, 319.0554.

5-**2d**: (77.1 mg, 26%), yellow oil; ^{1}H NMR: δ 7.57 (dd, J = 8.0, 1.5 Hz, 1H), 7.38 (d, J = 1.6 Hz, 1H), 6.57 (d, J = 8.0 Hz, 1H), 5.48 (dd, J = 6.8, 5.3 Hz, 1H), 5.00 (dd, J = 8.4, 5.1 Hz, 1H), 4.32 (q, J = 7.1 Hz, 2H), 3.20 (dd, J = 10.7, 5.3 Hz, 1H), 2.90 (ddd, J = 13.6, 8.4, 6.7 Hz, 1H), 2.82 (dd, J = 10.7, 6.9 Hz, 1H), 2.73 (ddd, J = 13.7, 10.2, 5.1 Hz, 1H), 1.88 (dd, J = 10.2, 6.7 Hz, 1H), 1.36 (t, J = 7.1 Hz, 3H); ^{13}C NMR: δ 166.8, 142.9, 139.7, 125.6, 122.8, 110.5, 108.4, 83.6, 72.0, 60.7, 39.4, 33.6, 14.6; IR (NaCl) ν: 2980, 2920, 1700, 1602, 1492, 1455, 1366, 1288, 1210, 1115, 1020, 765 cm^{-1}; HRMS (ESI) m/z: calcd for $C_{13}H_{16}N_2NaO_2S_2$ [M + Na]$^+$ 319.0545; found, 319.0554.

*(6-Nitro-3a,4-dihydro-1H,3H-benzo[4,5]imidazo[1,2-c]-thiazol-1-yl)methanethiol (4-**2e**) and (7-Nitro-3a,4-dihydro-1H,3H-benzo[4,5]imidazo[1,2-c]thiazol-1-yl)methanethiol (5-**2e**).* Prepared starting from 4-nitro-*o*-phenylenediamine (150 mg, 1 mmol) and purified with *n*-hexanes/EtOAc 8:2 to give a mixture of isomers 4-**2e** and 5-**2e** 0.223 g, 83%, (3:7).

4-**2e**: (59.2 mg, 22%): red solid; mp 206−208 °C; ^{1}H NMR 7.80 (dd, J = 8.5, 2.2 Hz, 1H), 7.43 (d, J = 2.2 Hz, 1H), 6.74

https://doi.org/10.1021/acsomega.3c03223
ACS Omega 2023, 8, 42114−42125

(d, J = 8.5 Hz, 2H), 5.54 (t, J = 6.0 Hz, 1H), 4.99 (dd, J = 8.8, 4.6 Hz, 1H), 4.59 (br, 1H), 3.22 (dd, J = 10.6, 5.2 Hz, 1H), 2.90 (dt, J = 8.8, 7.0 Hz, 1H), 2.84 (dd, J = 10.6, 7.9 Hz, 1H), 2.75 (ddd, J = 14.0, 10.5, 4.6 Hz, 1H), 1.83 (dd, J = 10.5, 6.8 Hz, 1H); ^{13}C NMR: δ 146.0, 142.6, 138.9, 119.5, 107.3, 105.0, 83.4, 69.4, 38.9, 33.4; IR (NaCl) ν: 1603, 1489, 1447, 1400, 1364, 1317, 1281, 1130, 1072, 858, 741 cm^{-1}; HRMS (ESI) m/z: calcd for $C_{10}H_{12}N_3NaO_2S_2$ $[M + H]^+$ 270.0365; found, 270.0366.

5-**2e**: (132 mg, 49%): orange solid; mp 128−134 °C; ^{1}H NMR: δ 7.81 (dd, J = 8.5, 2.2 Hz, 1H), 7.58 (d, J = 2.2 Hz, 1H), 6.51 (d, J = 8.5 Hz, 1H), 5.62 (ddd, J = 6.7, 5.1, 1.5 Hz, 1H), 4.97 (dd, J = 8.5, 4.9 Hz, 1H), 4.92 (br, 1H), 3.28 (dd, J = 10.8, 5.2 Hz, 1H), 2.90 (m, 2H), 2.77 (ddd, J = 13.9, 10.2, 4.9 Hz, 1H), 1.87 (dd, J = 10.2, 6.9 Hz, 1H); ^{13}C NMR: δ 144.8, 141.5, 140.0, 120.8, 106.4, 105.0, 84.0, 71.9, 39.5, 33.4; IR (NaCl) ν: 1600, 1490, 1446, 1400, 1362, 1318, 1280, 1130, 1075, 858, 740 cm^{-1}; HRMS (ESI) m/z: calcd for $C_{10}H_{12}N_3NaO_2S_2$ $[M + H]^+$ 270.0365; found, 270.0366.

*(6-Fluoro-3a,4-dihydro-1H,3H-benzo[4,5]imidazo[1,2-c]-thiazol-1-yl)methanethiol (4-**2f**) and (7-Fluoro-3a,4-dihydro-1H,3H-benzo[4,5]imidazo[1,2-c]thiazol-1-yl)-methanethiol (5-**2f**).* Prepared starting from 4-fluoro-1,2-phenylenediamine (126 mg, 1 mmol) and purified with *n*-hexanes/EtOAc 8:2 to give a mixture of isomers 4-**2f** and 5-**2f**, 0.182 g, 75%, (7:3).

4-**2f**: (94.5 mg, 39%): red solid; mp 82−85 °C; ^{1}H NMR: δ 6.66 (dd, J = 8.4, 4.7 Hz, 1H), 6.47 (td, J = 9.4, 2.4 Hz, 1H), 6.38 (dd, J = 8.8, 2.4 Hz, 1H), 5.39 (t, J = 6.0 Hz, 1H), 4.86 (dd, J = 9.0, 4.7 Hz, 1H), 4.28 (br, 1H), 3.18 (dd, J = 10.8, 5.3 Hz, 1H), 2.85 (m, 2H), 2.68 (ddd, J = 13.7, 10.4, 4.7 Hz, 1H), 1.90 (dd, J = 10.4, 6.4 Hz, 1H); ^{13}C NMR: δ 159.17 (d, J = 237.2 Hz), 139.51 (d, J = 12.0 Hz), 136.56 (d, J = 1.7 Hz), 109.84 (d, J = 9.8 Hz), 106.40 (d, J = 23.6 Hz), 99.30 (d, J = 28.0 Hz), 84.0, 72.7, 39.2, 33.7; IR (NaCl) ν: 1614, 1491, 1391, 1354, 1310, 1273, 1255, 1134, 833, 795 cm^{-1}; HRMS (ESI) m/z: calcd for $C_{10}H_{12}FN_2S_2$ $[M + H]^+$ 243.0426; found, 243.0404.

5-**2f**: (60.6 mg, 25%): orange oil; ^{1}H NMR: δ 6.62 (dd, J = 8.3, 4.7 Hz, 1H), 6.54 (dd, J = 9.0, 2.4 Hz, 1H), 6.46 (ddd, J = 9.3, 8.4, 2.5 Hz, 1H), 5.35 (dd, J = 7.9, 5.5 Hz, 1H), 4.89 (dd, J = 9.0, 4.5 Hz, 1H), 3.14 (dd, J = 10.7, 5.4 Hz, 1H), 2.88 (ddd, J = 13.2, 8.7, 6.2 Hz, 1H), 2.82 (dd, J = 10.6, 7.8 Hz, 1H), 2.70 (ddd, J = 13.8, 10.5, 4.5 Hz, 1H), 1.86 (dd, J = 10.5, 6.4 Hz, 1H); ^{13}C NMR: δ 159.6 (d, J = 238.0 Hz), 142.9 (d, J = 11.7 Hz), 133.8 (d, J = 1.8 Hz), 112.7 (d, J = 9.7 Hz), 107.0 (d, J = 23.5 Hz), 98.6 (d, J = 28.5 Hz), 83.9, 70.9, 38.5, 33.7; IR (NaCl) ν: 1610, 1490, 1390, 1314, 1272, 1255, 1130, 834, 785 cm^{-1}; HRMS (ESI) m/z: calcd for $C_{10}H_{12}FN_2S_2$ $[M + H]^+$ 243.0426; found, 243.0404.

*(7-Bromo-3a,4-dihydro-1H,3H-benzo[4,5]imidazo[1,2-c]-thiazol-1-yl)methanethiol (4-**2g**) and (6-Bromo-3a,4-dihydro-1H,3H-benzo[4,5]imidazo[1,2-c]thiazol-1-yl)-methanethiol (5-**2g**).* Prepared starting from 4-bromo-1,2-diaminobenzene (190 mg, 1 mmol) and purified with *n*-hexanes/EtOAc 8:2 to give a mixture of isomers 4-**2g** and 5-**2g** 0.209 g, 69%, (7:3).

4-**2g**: 109.2 mg; 36%, white solid; mp 146−152 °C; ^{1}H NMR: δ 6.90 (dd, J = 8.1, 1.8 Hz, 1H), 6.75 (d, J = 1.8 Hz, 1H), 6.63 (d, J = 8.1 Hz, 1H), 5.37 (dd, J = 7.1, 5.4 Hz, 1H), 4.88 (dd, J = 8.9, 4.6 Hz, 1H), 4.26 (br, 1H), 3.17 (dd, J = 10.7, 5.3 Hz, 1H), 2.87 (ddd, J = 13.0, 8.5, 6.0 Hz, 1H), 2.82 (dd, J = 10.8, 7.2 Hz, 1H), 2.68 (ddd, J = 13.7, 10.5, 4.7 Hz, 1H), 1.87 (dd, J = 10.5, 6.4 Hz, 1H); ^{13}C NMR: δ 139.8, 139.8, 123.9, 114.0, 113.7, 110.9, 83.5, 71.7, 39.1, 33.7; IR (NaCl) ν: 3362, 2930, 2543, 1603, 1482, 1422, 1401, 1297, 1246, 1218, 1060, 1001, 964, 907, 847, 797, 758, 696, 619 cm^{-1}; HRMS (ESI) m/z: calcd for $C_{10}H_{12}BrN_2S_2$ $[M + H]^+$ 302.9625; found, 302.9483.

5-**2g**: 57.6 mg; 19%; white solid; mp 102−105 °C; ^{1}H NMR: δ 6.88 (m, 2H), 6.52 (m, 1H), 5.37 (dd, J = 7.5, 5.4 Hz, 1H), 4.89 (dd, J = 8.9, 4.6 Hz, 1H), 4.17 (br, 1H), 3.16 (dd, J = 10.7, 5.3 Hz, 1H), 2.88 (ddd, J = 14.1, 9.1, 6.6 Hz, 1H), 2.82 (dd, J = 10.7, 7.6 Hz, 1H), 2.69 (ddd, J = 13.8, 10.6, 4.6 Hz, 1H), 1.86 (dd, J = 10.5, 6.5 Hz, 1H); ^{13}C NMR: δ 142.4, 137.5, 124.3, 113.7, 113.1, 112.5, 83.5, 71.2, 38.9, 33.7; IR (NaCl) ν: 3360, 2920, 2540, 1630, 1480, 1420, 1408, 1298, 1240, 1215, 1063, 1010, 961, 908, 847, 797, 760, 696, 620 cm^{-1}; HRMS (ESI) m/z: calcd for $C_{10}H_{12}BrN_2S_2$ $[M + H]^+$ 302.9625; found, 302.9483.

*Synthesis of S-(((1R,3aR)-3a,4-Dihydro-1H,3H-benzo[4,5]-imidazo[1,2-c]thiazol-1-yl)methyl) 4-Chlorobenzothioate (**7**).* To a stirred solution of *p*-chlorobenzoic acid (62 mg, 0.4 mmol) in CH_2Cl_2 dry (8 mL) were added HBTU (163 mg, 0.43 mmol), DIPEA (189 μL, 1.08 mmol), and 4-DMAP (4 mg, 0.036 mmol) y (±)-**2a** (80 mg, 0.36 mmol) at 0 °C. The mixture was stirred at rt for 2 h. The crude was poured into water (30 mL), extracted with EtOAc (3 × 50 mL), dried (Na_2SO_4), and filtered. The organic layer was evaporated under reduced pressure. The crude reaction mixture was purified by column chromatography on flash silica gel using *n*-hexanes/EtOAc (7:3) to give **7** (55 mg, 42%): green solid; mp 121−126 °C; ^{1}H NMR: δ 7.94 (m, 2H), 7.43 (m, 2H), 6.78 (m, 2H), 6.66 (m, 2H), 5.43 (ddd, J = 7.3, 5.2, 1.8 Hz, 1H), 5.05 (dd, J = 8.5, 5.7 Hz, 1H), 3.44 (m, 2H), 3.22 (ddd, J = 10.8, 5.5, 1.5 Hz, 1H), 2.85 (ddd, J = 11.0, 7.2, 1.4 Hz, 1H); ^{13}C RMN: δ 190.3, 140.7, 140.2, 138.2, 135.2, 129.1, 128.9, 121.9, 111.9, 109.9, 83.3, 68.5, 39.2, 37.9. IR (NaCl) ν: 3053, 2928, 1665, 1485, 1203, 916 cm^{-1}

Biocatalytic Assays. *General Procedure for the Analytical-Scale Screening.* In a 15 mL Falcon tube was added TBIM **2a** (0.05 mmol) dissolved in an appropriate solvent (500 μL), BH_3NH_3 (0.2 mmol, 4 equiv), and potassium phosphate buffer (10 mL, 0.1 M, pH = 7). Cell pellet (500 mg) from *E. coli* cultures expressing a MAO-N, corresponding to the D5, D9, and D11 variants were expressed as previously reported,[32] was added to the solution. The tube was placed in a shaking incubator and shaken at 37 °C and 250 rpm. The samples were prepared as follows: aqueous NaCl solution was added to a 1000 μL sample of the reaction mixture in a test tube, followed by 1 mL of EtOAc. After vigorous mixing by a vortex mixer, the organic phase was separated, dried with $MgSO_4$, and concentrated. Then, the residue was taken in DMSO (50 μL), *i*PrOH (450 μL), and *n*-hexanes (500 μL) and analyzed by chiral HPLC (DAICEL Chiralpak IF, 250 mm × 4.6 mm, 5 μm column; flow rate 1 mL/min; λ 306 nm; eluent = *n*-hexanes/*i*PrOH 8:2; Rt [(*R*,*R*)] = 7.3 min, Rt [(*S*,*S*)] = 9.4 min).

2b: *n*-hexanes/*i*PrOH 8:2; λ 306 nm, t_1 = 14.8 min, and t_2 = 17.8 min.

4-**2c**: *n*-hexanes/*i*PrOH 8:2; λ 312 nm, t_1 = 8.0 min, and t_2 = 9.6 min.

5-**2c**: *n*-hexanes/*i*PrOH 8:2; λ 312 nm, t_1 = 8.1 min, and t_2 = 9.8 min.

4-**2d**: *n*-hexanes/*i*PrOH 6:4; λ 330 nm, t_1 = 6.7 min, and t_2 = 19.0 min.

https://doi.org/10.1021/acsomega.3c03223
ACS Omega 2023, 8, 42114−42125

5-**2d**: *n*-hexanes/*i*PrOH 6:4; λ 330 nm, t_1 = 6.8 min, and t_2 = 10.6 min.

4-**2e**: *n*-hexanes/*i*PrOH 6:4; λ 306 nm, t_1 = 14.2 min, and t_2 = 21.3 min.

5-**2e**: *n*-hexanes/*i*PrOH 6:4; λ 306 nm, t_1 = 9.0 min, and t_2 = 13.5 min.

4-**2f**: *n*-hexanes/*i*PrOH 8:2; λ 313 nm, t_1 = 7.9 min, and t_2 = 8.6 min.

5-**2f**: *n*-hexanes/*i*PrOH 8:2; λ 315 nm, t_1 = 8.6 min, and t_2 = 11.5 min.

4-**2g**: *n*-hexanes/*i*PrOH 8:2; λ 318 nm, t_1 = 8.4 min, and t_2 = 10.1 min.

5-**2g**: *n*-hexanes/*i*PrOH 8:2; λ 318 nm, t_1 = 9.1 min, and t_2 = 15.1 min.

Preparative Procedure. In a 250 mL Erlenmeyer flask was added TBIM **2a** (0.45 mmol) dissolved in DMF (5 mL), BH_3NH_3 (0.2 mmol, 4 equiv), and potassium phosphate buffer (10 mL, 0.1 M, pH = 7). Cell pellets (500 mg) from *E. coli* cultures containing MAO-N D11 were added to the solution. The tube was placed in a shaking incubator and shaken at 37 °C and 250 rpm. The crude was poured into a saturated NaCl solution (1 mL) and extracted with EtOAc (3 × 1 mL). The organic layer was evaporated under reduced pressure and purified by SiO_2 column chromatography, eluent *n*-hexanes/EtOAc (8:2) to give (+)-**2a** (35 mg, 35%, 89% ee, α_D = +90°) and (−)-**6** (5 mg, 5%).

*(S)-(1H,3H-Benzo[4,5]imidazo[1,2-c]thiazol-1-yl)-methanethiol (−)-**6**.* ^{1}H RMN: δ 7.73 (dd, J = 6.1, 2.2 Hz, 1H), 7.35 (dd, J = 5.5, 2.2 Hz, 1H), 7.28 (m, 2H), 5.78 (ddd, J = 5.5, 3.1, 1.9 Hz, 1H), 4.44 (dd, J = 14.6, 1.9 Hz, 1H), 4.16 (d, J = 14.5 Hz, 1H), 3.23 (m, 2H), 1.50 (t, J = 8.9 Hz, 1H); ^{13}C RMN: δ 158.2, 149.1, 131.6, 122.8, 122.7, 120.5, 109.5, 62.0, 32.2, 27.9. $[\alpha]_D^{20}$ = −55.6 (CH_2Cl_2, c = 0.21); IR (NaCl) ν: 2922, 2555, 1616, 1525, 1454, 741 cm^{-1} HRMS (ESI) m/z: calcd for $C_{10}H_{11}N_2S_2$ $[M + H]^+$ 223.0364; found, 223.0366.

Optical Rotation and ECD Spectra Computational Predictions. *SS* and *RR* enantiomer structures were built in MOE2019 (Chemical Computing Group ULC). A stochastic conformational search was performed in the MOE over both enantiomers. Dichloromethane was used as a simulated solvent for the conformational search through a generalized Born implicit solvation model (ε = 8.93). All conformations within an energy window of 7 kcal/mol, as estimated with (AMBER14:EHT force field[45]), and RMSD > 0.25 Å were retained. Conformational analysis showed that the structure is very rigid, with the thiol bond free rotation being the only variation among the different conformations. The three conformations with lowest energy for each enantiomer were used as input for density functional theory (DFT) calculations.[46] Optimization and frequency calculations were performed in Gaussian16 using the ub3lyp functional[47] and 6-31++g(d,p) basis set, with an ultrafine integration grid and no symmetry constraints. Implicit solvation (dichloromethane for optical rotation and chloroform for ECD spectra, to match the experimental conditions) was simulated by an IEFPCM method, with radii and non-electrostatic terms from Truhlar and co-workers' SMD solvation model.[48] Optical rotation was calculated at 589.3 nm from DFT-optimized structures.[49] For ECD spectra calculations, a time-dependent DFT calculation[50] was performed with the same functional and basis set in order to get 30 excited states and their electronic transition intensities and rotatory strengths.

HPLC Method. A chiral phase separation column was used (DAICEL Chiralpak IF, 250 mm × 4.6 mm, 5 μm). Measurements were carried out under isocratic conditions. The eluent consisted of *n*-hexanes (mobile phase A) and isopropanol (mobile phase B) at a flow rate of 1.0 mL/min. The injection volume was 20 μL. Data and chromatograms were collected and analyzed using the Empower System program from Waters Corporation, 2002. Retention times and isocratic conditions are available in the Supporting Information.

% Yields. Yields were calculated using an external standard (Std 1) and corrected using a recovering factor, calculated as follows:

(a) External standard preparation (Std 1): TBIM (50 μL of a solution 90 mM in DMSO) was diluted in *i*PrOH (450 μL) and *n*-hexanes (500 μL). The solution was filtered and analyzed by chiral HPLC.

(b) Standard inoculated into inactivated cells (Std 2): TBIM (50 μL of a solution 90 mM in DMSO) was suspended in EtOAc (1 mL) and it was added an *E. coli* culture containing a MAO-N D11 suspension (1 mL). After vigorous mixing by a vortex mixer, the organic phase was separated, dried with $MgSO_4$, and concentrated. Then, the residue was taken in DMSO (50 μL) and added isOH (450 μL) and *n*-hexanes (500 μL) and analyzed by chiral HPLC.

(c) Recovering factor (F) = $A_{(Std2)}/A_{(Std1)}$.

$$\%\ \text{Yield} = A_{\text{Enantiomer}}/A_{(\text{Std1})} \times (1/F)$$

Recovering factors are available in Table S3.

ECD Experiments. In a 2 mL vial, was dissolved (+)-**2a** in $CHCl_3$ (300 μL), and then diluted with $CHCl_3$ (final concentration = 9,75 × 10^{-6} M). The ECD spectrum was recorded in the range 230−400 nm using $CHCl_3$ as the reference. The data obtained (θ, mdeg) were converted into ΔA according to[44]

$$\theta\ (\text{deg}) = 32.98 \cdot \Delta A \times 1000$$

Then, the $\Delta\varepsilon$ was calculated according to

$$\Delta A = \Delta\varepsilon \times c \times [\mathbf{2a}]$$

where c = 1 cm and [**2a**] = 9,75 × 10^{-6} M.

Data available in the Supporting Information.

In Silico Reconstruction and Relaxation of Missing Structural Regions in MAO-N D11. The amino acid sequence of the full MAO-N D11 (495 residues) was aligned to the crystal structure (PDB code 3zdn, chains A and B) and a 3D model was created with MODELLER[51] to rebuild the regions not defined in the electron density map. Protonation states at pH 7.8 were assigned by the PDB2PQR server.[52] The FAD cofactor was added as found in the crystal structure; the model was neutralized with 12 K^+ ions, solvated with explicit waters and 1 M KCl, and minimized in solution. Then, it was thermalized to 310 K at *NVT* and simulated during 100 ns by employing MD at *NPT* (P = 1 bar). To treat the protein the ff19SB force field[53] was used, and the entire system was surrounded by a truncated octahedral box of TIP3P water molecules,[54] applying Dang's parameters on ions.[55] The FAD cofactor was treated with the parameters found in the RED database.[56] All systems were simulated by using the Langevin algorithm to control the temperature and the pressure, with a coupling constant of 5 ps. SHAKE was used to keep all bonds

https://doi.org/10.1021/acsomega.3c03223
ACS Omega 2023, 8, 42114−42125

involving hydrogen at their equilibrium values, which allowed us to use a 2 fs step for the integration of Newtons equations of motion. Long-range electrostatic interactions were accounted for using the Particle Mesh Ewald method with standard defaults. All simulations were carried out using the PMEMD CUDA code module of AMBER18 and analyzed with CPPTRAJ.[57] Data of RMSD and RMSF are available in Figures S18 and S19.

Docking of Substrate 1 and MD Simulations. Ligands were initially prepared using YASARA's molecular modeling software. Solvation of the ligands was performed in an explicit solvent shell at pH 7.4 and a 0.9% NaCl concentration prior to energy minimization. Energy minimization was performed to refine the bond lengths and angles of the ligands. The minimized conformation with the lowest energy for each ligand was used in the docking experiments.

Flexible docking was performed using AutoDock VINA software with default parameters but with the number of VINA runs increased to 250. The size of the docking box was set to 5 Å around the amino acids in the active site of each protein structure. Clusters were generated based on positions with a root-mean-square deviation (RMSD) lower than 2.5 Å and were represented by the position with the lowest free energy of binding.

Every cluster generated by AutoDock VINA for each substrate used in amine oxidation was analyzed. The binding energy, distance for hydride transfer from FAD, and interactions were evaluated.

The best scoring docking structures for both the *SS* and *RR* enantiomers were subjected to two different 100 ns MD simulations in equal conditions as the above indicated, but one of them using a harmonic potential of 1.5 kcal/mol/Å^2 to steer the substrate toward the FAD cofactor to reach the reaction distance. Both simulations were clustered and MM-GBSA/PBSA calculations were performed. Data are available in Table S5.

■ ASSOCIATED CONTENT

Supporting Information

The Supporting Information is available free of charge at https://pubs.acs.org/doi/10.1021/acsomega.3c03223.

Full spectroscopic data and copies of ^{1}H NMR and ^{13}C NMR spectra and crystal structure of compound **7** (PDF)

■ AUTHOR INFORMATION

Corresponding Authors

César Iglesias − *Departamento de Biociencias, Laboratorio de Microbiología Molecular, Facultad de Quimica and Departamento de Biociencias y Departamento de Quimica Organica, Laboratorio de Biocatalisis y Biotransformaciones, Facultad de Quimica, Universidad de la Republica, Montevideo, Montevideo 11800, Uruguay;* orcid.org/0000-0002-9438-4572; Email: ciglesias@fq.edu.uy

Graciela Mahler − *Departamento de Química Orgánica, Laboratorio de Quimica Farmaceutica, Facultad de Quimica, Universidad de la República, Montevideo, Montevideo 11800, Uruguay;* orcid.org/0000-0003-0612-0516; Email: gmahler@fq.edu.uy

Authors

Valentina Villamil − *Departamento de Química Orgánica, Laboratorio de Quimica Farmaceutica, Facultad de Quimica, Universidad de la República, Montevideo, Montevideo 11800, Uruguay*

Franco Vairoletti − *Departamento de Química Orgánica, Laboratorio de Quimica Farmaceutica, Facultad de Quimica, Universidad de la República, Montevideo, Montevideo 11800, Uruguay; Programa de Posgrado en Quimica, Universidad de la República Uruguay, Montevideo, Montevideo 11800, Uruguay;* orcid.org/0000-0002-5160-2250

Ariel Tijman − *Programa de Posgrado en Quimica, Universidad de la República Uruguay, Montevideo, Montevideo 11800, Uruguay; Departamento de Biociencias, Laboratorio de Microbiología Molecular, Facultad de Quimica and Departamento de Biociencias y Departamento de Quimica Organica, Laboratorio de Biocatalisis y Biotransformaciones, Facultad de Quimica, Universidad de la Republica, Montevideo, Montevideo 11800, Uruguay;* orcid.org/0000-0003-3308-1110

Gonzalo López − *Programa de Posgrado en Quimica, Universidad de la República Uruguay, Montevideo, Montevideo 11800, Uruguay; Departamento de Biociencias, Laboratorio de Microbiología Molecular, Facultad de Quimica and Departamento de Biociencias y Departamento de Quimica Organica, Laboratorio de Biocatalisis y Biotransformaciones, Facultad de Quimica, Universidad de la Republica, Montevideo, Montevideo 11800, Uruguay*

Alejandro Peixoto de Abreu Lima − *Departamento de Química Orgánica, Laboratorio de Síntesis Orgánica, Facultad de Quimica, Universidad de la Republica, Montevideo, Montevideo 11800, Uruguay*

Cecilia Saiz − *Departamento de Química Orgánica, Laboratorio de Quimica Farmaceutica, Facultad de Quimica, Universidad de la República, Montevideo, Montevideo 11800, Uruguay;* orcid.org/0000-0002-6451-1366

Complete contact information is available at: https://pubs.acs.org/10.1021/acsomega.3c03223

Notes

The authors declare no competing financial interest.

■ ACKNOWLEDGMENTS

This work was supported partially by the National Institute of Allergy and Infectious Diseases of the National Institutes of Health (NIH) to G.M. under award number R01AI100560, Centro CEIBOS Espacio Interdisciplinario, Udelar; CSIC, Udelar and Agencia NacionaI de Investigación e Innovación Uruguay (ANII) (FCE_3_2022_1_172465) to C.I. A.T., V.V., and F.V. are recipients of a fellowship from CAP UdelaR. Prof. Nicholas Turner is acknowledged for kindly supplying MAO-N enzymes. Prof. Martin Flo is acknowledged for the circular dichroism spectra. Graphical abstract created with http://biorender.com/.

■ REFERENCES

(1) Singh, P.; Varshnaya, R. K.; Dey, R.; Banerjee, P. Donor-Acceptor Cyclopropanes as an Expedient Building Block Towards the Construction of Nitrogen-Containing Molecules: An Update. *Adv. Synth. Catal.* **2020**, *362* (7), 1447−1484.

(2) Didehban, K.; Vessally, E.; Salary, M.; Edjlali, L.; Babazadeh, M. Synthesis of a Variety of Key Medicinal Heterocyclic Compounds via

Chemical Fixation of CO2 onto O-Alkynylaniline Derivatives. *J. CO2 Util.* **2018**, *23*, 42−50.
(3) Hossain, M. A Review on Heterocyclic: Synthesis and Their Application in Medicinal Chemistry of Imidazole Moiety. *Sci. J. Chem.* **2018**, *6* (5), 83.
(4) Liu, H.; Du, D. M. Recent Advances in the Synthesis of 2-Imidazolines and Their Applications in Homogeneous Catalysis. *Adv. Synth. Catal.* **2009**, *351* (4), 489−519.
(5) Tyagi, R.; Tyagi, V. K.; Pandey, S. K. Imidazoline and Its Derivatives: An Overview. *J. Oleo Sci.* **2007**, *56* (5), 211−222.
(6) Frishman, H. Nervous System in Regulating Vasomotor **1996**, *36* (2), 98−111.
(7) Jou, S. B.; Liu, I. M.; Cheng, J. T. Activation of Imidazoline Receptor by Agmatine to Lower Plasma Glucose in Streptozotocin-Induced Diabetic Rats. *Neurosci. Lett.* **2004**, *358* (2), 111−114.
(8) Halaris, A.; Piletz, J. E. Relevance of Imidazoline Receptors and Agmatine to Psychiatry: A Decade of Progress. *Ann. N.Y. Acad. Sci.* **2003**, *1009*, 1−20.
(9) Chikashita, H.; Ide, H.; Itoh, K. 1,3-Dimethyl-2-phenylbenzimidazoline as a novel and efficient reagent for mild reductive dehalogenation of .alpha.-halo carbonyl compounds and acid chlorides. *J. Org. Chem.* **1986**, *51* (26), 5400−5405.
(10) Mahesh Reddy, G.; Reddy, P. S. N. Antibacterial Activity of Some N, N'-Linked Bisazaheterocycles, Benzimidazoline and Quinoxaline Derivatives. *Rasayan J. Chem.* **2008**, *1* (1), 179−184.
(11) Alizadeh, A.; Bagherinejad, A.; Moafi, L.; Zhu, L. G. A Catalyst-Free Synthetic Route to Thiazolo[3,4- a]Benzimidazole Derivatives through a Three-Component Reaction. *Synlett* **2016**, *27* (12), 1803−1805.
(12) Saiz, C.; Castillo, V.; Fontán, P.; Bonilla, M.; Salinas, G.; Rodríguez-Haralambides, A.; Mahler, S. G. Discovering Echinococcus Granulosus Thioredoxin Glutathione Reductase Inhibitors through Site-Specific Dynamic Combinatorial Chemistry. *Mol. Diversity* **2014**, *18* (1), 1−12.
(13) Martínez, V.; Villamil, V.; Duarte, D.; Saiz, C.; Davyt, D.; Fontana, C.; Veiga, N.; Mahler, G. Preparation and Mechanistic Studies of 2-Substituted Bisthiazolidines by Imine Exchange. *Eur. J. Org Chem.* **2020**, *2020* (9), 1084−1092.
(14) Alkadi, H.; Jbeily, R. Role of Chirality in Drugs: An Overview. *Infect. Disord. - Drug Targets* **2018**, *18* (2), 88−95.
(15) Ghislieri, D.; Turner, N. J. Biocatalytic Approaches to the Synthesis of Enantiomerically Pure Chiral Amines. *Top. Catal.* **2014**, *57* (5), 284−300.
(16) Kohls, H.; Steffen-Munsberg, F.; Höhne, M. Recent Achievements in Developing the Biocatalytic Toolbox for Chiral Amine Synthesis. *Curr. Opin. Chem. Biol.* **2014**, *19* (1), 180−192.
(17) Grogan, G. Synthesis of Chiral Amines Using Redox Biocatalysis. *Curr. Opin. Chem. Biol.* **2018**, *43*, 15−22.
(18) Kelly, S. A.; Pohle, S.; Wharry, S.; Mix, S.; Allen, C. C. R.; Moody, T. S.; Gilmore, B. F. Application of ω-Transaminases in the Pharmaceutical Industry. *Chem. Rev.* **2018**, *118* (1), 349−367.
(19) O'Reilly, E.; Iglesias, C.; Turner, N. J. Monoamine Oxidase−ω-Transaminase Cascade for the Deracemisation and Dealkylation of Amines. *ChemCatChem* **2014**, *6* (4), 992−995.
(20) Batista, V. F.; Galman, J. L.; G A Pinto, D. C.; Silva, A. M. S.; Turner, N. J. Monoamine Oxidase: Tunable Activity for Amine Resolution and Functionalization. *ACS Catal.* **2018**, *8* (12), 11889−11907.
(21) Li, T.; Liang, J.; Ambrogelly, A.; Brennan, T.; Gloor, G.; Huisman, G.; Lalonde, J.; Lekhal, A.; Mijts, B.; Muley, S.; Newman, L.; Tobin, M.; Wong, G.; Zaks, A.; Zhang, X. Efficient, Chemoenzymatic Process for Manufacture of the Boceprevir Bicyclic [3.1.0]Proline Intermediate Based on Amine Oxidase-Catalyzed Desymmetrization. *J. Am. Chem. Soc.* **2012**, *134* (14), 6467−6472.
(22) McIntosh, J. A.; Coelho, P. S.; Farwell, C. C.; Wang, Z. J.; Lewis, J. C.; Brown, T. R.; Arnold, F. H. Enantioselective Intramolecular C-H Amination Catalyzed by Engineered Cytochrome P450 Enzymes in Vitro and in Vivo. *Angew. Chem., Int. Ed.* **2013**, *52* (35), 9309−9312.
(23) Dydio, P.; Key, H. M.; Hayashi, H.; Clark, D. S.; Hartwig, J. F. Chemoselective, Enzymatic C-H Bond Amination Catalyzed by a Cytochrome P450 Containing an Ir(Me)-PIX Cofactor. *J. Am. Chem. Soc.* **2017**, *139* (5), 1750−1753.
(24) Chen, F. F.; Cosgrove, S. C.; Birmingham, W. R.; Mangas-Sanchez, J.; Citoler, J.; Thompson, M. P.; Zheng, G. W.; Xu, J. H.; Turner, N. J. Enantioselective Synthesis of Chiral Vicinal Amino Alcohols Using Amine Dehydrogenases. *ACS Catal.* **2019**, *9* (12), 11813−11818.
(25) Abrahamson, M. J.; Vázquez-Figueroa, E.; Woodall, N. B.; Moore, J. C.; Bommarius, A. S. Development of an Amine Dehydrogenase for Synthesis of Chiral Amines. *Angew. Chem., Int. Ed.* **2012**, *51* (16), 3969−3972.
(26) Patil, M. D.; Grogan, G.; Bommarius, A.; Yun, H. Oxidoreductase-Catalyzed Synthesis of Chiral Amines. *ACS Catal.* **2018**, *8* (12), 10985−11015.
(27) Mangas-Sanchez, J.; France, S. P.; Montgomery, S. L.; Aleku, G. A.; Man, H.; Sharma, M.; Ramsden, J. I.; Grogan, G.; Turner, N. J. Imine Reductases (IREDs). *Curr. Opin. Chem. Biol.* **2017**, *37*, 19−25.
(28) Aleku, G. A.; France, S. P.; Man, H.; Mangas-Sanchez, J.; Montgomery, S. L.; Sharma, M.; Leipold, F.; Hussain, S.; Grogan, G.; Turner, N. J. A Reductive Aminase from Aspergillus Oryzae. *Nat. Chem.* **2017**, *9* (10), 961−969.
(29) Dunsmore, C. J.; Carr, R.; Fleming, T.; Turner, N. J. A Chemo-Enzymatic Route to Enantiomerically Pure Cyclic Tertiary Amines. *J. Am. Chem. Soc.* **2006**, *128* (7), 2224−2225.
(30) Ghislieri, D.; Houghton, D.; Green, A. P.; Willies, S. C.; Turner, N. J. Monoamine Oxidase (MAO-N) Catalyzed Deracemization of Tetrahydro-β- Carbolines: Substrate Dependent Switch in Enantioselectivity. *ACS Catal.* **2013**, *3* (12), 2869−2872.
(31) Ghislieri, D.; Green, A. P.; Pontini, M.; Willies, S. C.; Rowles, I.; Frank, A.; Grogan, G.; Turner, N. J. Engineering an Enantioselective Amine Oxidase for the Synthesis of Pharmaceutical Building Blocks and Alkaloid Natural Products. *J. Am. Chem. Soc.* **2013**, *135* (29), 10863−10869.
(32) Carr, R.; Alexeeva, M.; Dawson, M. J.; Gotor-Fernández, V.; Humphrey, C. E.; Turner, N. J. Directed Evolution of an Amine Oxidase for the Preparative Deracemisation of Cyclic Secondary Amines. *ChemBioChem* **2005**, *6* (4), 637−639.
(33) Atkin, K. E.; Reiss, R.; Turner, N. J.; Brzozowski, A. M.; Grogan, G. Cloning, Expression, Purification, Crystallization and Preliminary X-Ray Diffraction Analysis of Variants of Monoamine Oxidase from Aspergillus Niger. *Acta Crystallogr., Sect. F: Struct. Biol. Cryst. Commun.* **2008**, *64* (3), 182−185.
(34) Moshinsky, M. Transformation Brackets for Harmonic Oscillator Functions. *Nucl. Phys.* **1959**, *13* (1), 104−116.
(35) Rao, A.; Chimirri, A.; Ferro, S.; Monforte, A. M.; Monforte, P.; Zappalà, M. Microwave-induced synthesis of benzimidazole and thiazolidinone derivatives as HIV-1 RT inhibitors. *Arkivoc* **2004**, *2004* (5), 147−155.
(36) Soares, M. I. L.; Pinho e Melo, T. M. V. D. Synthesis and Thermal Reactivity of Thiazolo[3,4-a]Benzimidazole-2,2-Dioxides: Approach to 1H-Benzo[d]Imidazoles via Novel Benzo-2,5-Diazafulvenium Methides. *Tetrahedron* **2015**, *71* (24), 4227−4235.
(37) Chimirri, A.; Grasso, S.; Monforte, P.; Rao, A.; Zappalà, M.; Monforte, A. M.; Pannecouque, C.; Witvrouw, M.; Balzarini, J.; De Clercq, E. Synthesis and Biological Activity of Novel 1H,3H-Thiazolo[3,4-a]Benzimidazoles: Non-Nucleoside Human Immunodeficiency Virus Type 1 Reverse Transcriptase Inhibitors. *Antiviral Chem. Chemother.* **1999**, *10* (4), 211−217.
(38) Chajkowski-Scarry, S.; Rimoldi, J. M. Monoamine Oxidase A and B Substrates: Probing the Pathway for Drug Development. *Future Med. Chem.* **2014**, *6* (6), 697−717.
(39) Orru, R.; Aldeco, M.; Edmondson, D. E. Do MAO A and MAO B Utilize the Same Mechanism for the C-H Bond Cleavage Step in Catalysis? Evidence Suggesting Differing Mechanisms. *J. Neural Transm.* **2013**, *120* (6), 847−851.
(40) Silverman, R. B. Radical Ideas about Monoamine Oxidase. *Acc. Chem. Res.* **1995**, *28* (8), 335−342.

https://doi.org/10.1021/acsomega.3c03223
ACS Omega 2023, 8, 42114−42125

(41) Zhao, F.; Masci, D.; Ferla, S.; Varricchio, C.; Brancale, A.; Colonna, S.; Black, G. W.; Turner, N. J.; Castagnolo, D. Monoamine Oxidase (MAO-N) Biocatalyzed Synthesis of Indoles from Indolines Prepared via Photocatalytic Cyclization/Arylative Dearomatization. *ACS Catal.* **2020**, *10* (11), 6414−6421.
(42) Beilles, S.; Cardinael, P.; Ndzié, E.; Petit, S.; Coquerel, G. Preferential Crystallisation and Comparative Crystal Growth Study between Pure Enantiomer and Racemic Mixture of a Chiral Molecule: 5-Ethyl-5-Methylhydantoin. *Chem. Eng. Sci.* **2001**, *56* (7), 2281−2294.
(43) McCann, D. M.; Stephens, P. J.; Cheeseman, J. R. Determination of Absolute Configuration Using Density Functional Theory Calculation of Optical Rotation: Chiral Alkanes. *J. Org. Chem.* **2004**, *69* (25), 8709−8717.
(44) Evans, A. C.; Petit, A. S.; Guillen, S. G.; Neukirch, A. J.; Hoffmann, S. V.; Jones, N. C. Chiroptical Characterization Tools for Asymmetric Small Molecules-Experimental and Computational Approaches for Electronic Circular Dichroism (ECD) and Anisotropy Spectroscopy. *RSC Adv.* **2021**, *11* (3), 1635−1643.
(45) Maier, J. A.; Martinez, C.; Kasavajhala, K.; Wickstrom, L.; Hauser, K. E.; Simmerling, C. ff14SB: Improving the Accuracy of Protein Side Chain and Backbone Parameters from ff99SB. *J. Chem. Theory Comput.* **2015**, *11* (8), 3696−3713.
(46) Berger, R. Computational Chemistry. Introduction to the Theory and Applications of Molecular and Quantum Mechanics. By Errol G. Lewars. *Angew. Chemie Int. Ed.* **2004**, *43* (38), 4979−4980.
(47) Miehlich, B.; Savin, A.; Stoll, H.; Preuss, H. Results Obtained with the Correlation Energy Density Functionals of Becke and Lee, Yang and Parr. *Chem. Phys. Lett.* **1989**, *157* (3), 200−206.
(48) Marenich, A. V.; Cramer, C. J.; Truhlar, D. G. Universal Solvation Model Based on Solute Electron Density and on a Continuum Model of the Solvent Defined by the Bulk Dielectric Constant and Atomic Surface Tensions. *J. Phys. Chem. B* **2009**, *113* (18), 6378−6396.
(49) Stephens, P. J.; Devlin, F. J.; Cheeseman, J. R.; Frisch, M. J.; Bortolini, O.; Besse, P. Determination of Absolute Configuration Using Ab Initio Calculation of Optical Rotation. *Chirality* **2003**, *15*, 57−64.
(50) Adamo, C.; Jacquemin, D. The Calculations of Excited-State Properties with Time-Dependent Density Functional Theory. *Chem. Soc. Rev.* **2013**, *42* (3), 845−856.
(51) Šali, A.; Blundell, T. L. Comparative Protein Modelling by Satisfaction of Spatial Restraints. *J. Mol. Biol.* **1993**, *234* (3), 779−815.
(52) Jurrus, E.; Engel, D.; Star, K.; Monson, K.; Brandi, J.; Felberg, L. E.; Brookes, D. H.; Wilson, L.; Chen, J.; Liles, K.; Chun, M.; Li, P.; Gohara, D. W.; Dolinsky, T.; Konecny, R.; Koes, D. R.; Nielsen, J. E.; Head-Gordon, T.; Geng, W.; Krasny, R.; Wei, G. W.; Holst, M. J.; McCammon, J. A.; Baker, N. A. Improvements to the APBS Biomolecular Solvation Software Suite. *Protein Sci.* **2018**, *27* (1), 112−128.
(53) Tian, C.; Kasavajhala, K.; Belfon, K. A. A.; Raguette, L.; Huang, H.; Migues, A. N.; Bickel, J.; Wang, Y.; Pincay, J.; Wu, Q.; Simmerling, C. Ff19SB: Amino-Acid-Specific Protein Backbone Parameters Trained against Quantum Mechanics Energy Surfaces in Solution. *J. Chem. Theory Comput.* **2020**, *16* (1), 528−552.
(54) Jorgensen, W. L.; Chandrasekhar, J.; Madura, J. D.; Impey, R. W.; Klein, M. L. Comparison of Simple Potential Functions for Simulating Liquid Water. *J. Chem. Phys.* **1983**, *79* (2), 926−935.
(55) Smith, D. E.; Dang, L. X. Computer Simulations of NaCl Association in Polarizable Water. *J. Chem. Phys.* **1994**, *100* (5), 3757−3766.
(56) Dupradeau, F. Y.; Cezard, C.; Lelong, R.; Stanislawiak, E.; Pecher, J.; Delepine, J. C.; Cieplak, P. R.E.DD.B.: A Database for RESP and ESP Atomic Charges, and Force Field Libraries. *Nucleic Acids Res.* **2007**, *36*, 360−367.
(57) Case, D. A.; Aktulga, H. M.; Belfon, K.; Ben-Shalom, I. Y.; Berryman, J. T.; Brozell, S. R.; Cerutti, D. S.; Cheatham, T. E., III; G, A. C.; Cruzeiro, V. W. D.; Darden, T. A.; Duke, R. E.; Giambasu, G.; Gilson, M. K.; Gohlke, H.; Goetz, A. W.; Harris, R.; Izadi, S.; Izmailov, S. A.; Kasavajhala, K.; Kaymak, M. C.; King, E.; Kovalenko, A.; Kurtzman, T.; Lee, T. S.; LeGrand, S.; Li, P.; Lin, C.; Liu, J.; Luchko, T.; Luo, R.; Machado, M.; Man, V.; Manathunga, M.; Merz, K. M.; Miao, Y.; Mikhailovskii, O.; Monard, G.; Nguyen, H.; O'Hearn, K. A.; Onufriev, A.; Pan, F.; Pantano, S.; Qi, R.; Rahnamoun, A.; Roe, D. R.; Roitberg, A.; Sagui, C.; Schott-Verdugo, S.; Shajan, A.; Shen, J.; Simmerling, C. L.; Skrynnikov, N. R.; Smith, J.; Swails, J.; Walker, R. C.; Wang, J.; Wang, J.; Wei, H.; Wolf, R. M.; Wu, X.; Xiong, Y.; Xue, Y.; York, D. M.; Zhao, S.; Kollman, P. A. *Amber 2022*; University of California: San Francisco, 2022.

https://doi.org/10.1021/acsomega.3c03223
ACS Omega 2023, 8, 42114−42125